ChemComm

Accepted Manuscript

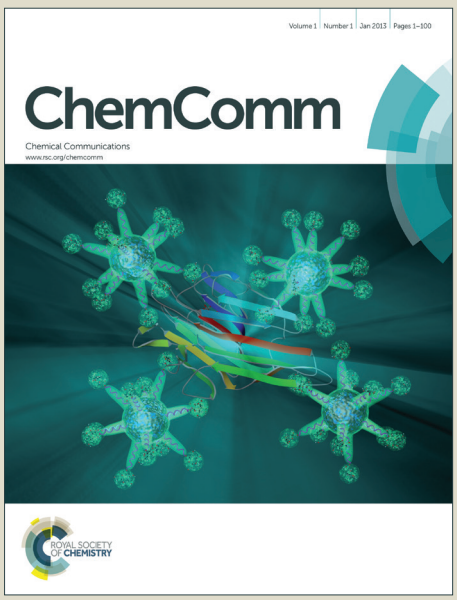

ROYAL SOCIETY OF CHEMISTRY

www.rsc.org/chemcomm

Journal Name RSCPublishing

COMMUNICATION

www.rsc.org/

Cite this: DOI: 10.1039/x0xx00000x

Received 00th January 2012,
Accepted 00th January 2012

DOI: 10.1039/x0xx00000x

Structural and electronic modification of MoS_2 nanosheets using S-doped carbon for efficient electrocatalysis of hydrogen evolution reaction

Thangavel Naresh Kumar[a], Naveen Chandrasekaran[b], Kanala Lakshminarasimha Phani*[a]

We discovered the in situ generation of S-doped carbon sandwiched between the MoS_2 nano-sheets during pyrolysis of Mo(VI)-polydopamine (PDA) in presence of elemental sulfur. This causes enrichment of MoS_2 with more edge planes (2H ⟶ 1T), also resulting in enhanced charge density and electronic conductivity. The phase transformed MoS_2[@S-C_{PDA}] exhibits enhanced HER activity with η =160 mV at a current density of 10 mA cm^{-2}.

Hydrogen represents one of the most promising clean energy sources[1]. For its efficient production through electrochemical hydrogen evolution reaction (HER), metal alloys[2], enzymes[3], metal dichalcogenides[4], metal oxides[5] and a few molecular electrocatalysts[6,7] have been reported. Molybdenum disulfide (MoS_2) promises an earth-abundant, low-cost alternative to the precious metals.[8] Considerable effort has been invested to investigate and optimize the catalytic activity of various MoS_2 materials in the form of nanoparticles[9], mesoporous forms[10,11], nanowires[12], amorphous and doped MoS_2 [13,14], thin solid films[13], graphene-supported MoS_2 heterostructures [15–17] and chemically exfoliated layers.[18,19] HER on bulk MoS_2 requires high overpotentials due to its poor intrinsic electronic conductivity and low crystallinity. It was later found that edge planes in MoS_2 have more unsaturated sulfur than the basal planes which are responsible for the increased activity towards hydrogen evolution reaction.[20] It was suggested that the edge site and metallic 1T polymorph of MoS_2 materials are catalytically active.[18,21] It has been recently shown that conversion of semiconducting 2H MoS_2 (trigonal prismatic) to metallic 1T (octahedral) phase improves the HER catalytic performance, but the mechanism responsible for the enhancement is presently not fully elucidated.[18] example, it is unclear if the enhancement in the catalyst properties is related to increased conductivity of the nano-sheets that can facilitate charge transfer kinetics or if the metastable metallic 1T phase of MoS_2 is intrinsically more active. Motivated by these findings, we reasoned that simultaneous increase in electrical conductivity and transformation of MoS_2 to its 1T phase will lead to an electrocatalyst with exceptional properties suitable for HER. In recent years, mussel-inspired adhesive surface coatings based on catecholamines such as dopamine, 3,4-dihydroxyphenylalanine (mimic of mytilusedulis foot protein Mefb-5) are attractive due to their adhesion to diverse substrates, biocompatibility etc.[22,23] These catecholamine based monomers undergo self-polymerization under mild alkaline conditions or chemical oxidation. The available knowledge suggests that the polymer is made up of polyindole units.[24,25] Polydopamines are used for simultaneous reduction and functionalization of carbon substrates such as graphene oxide[26], carbon nanotubes[27] (CNT) and used in energy storage/conversion device fabrication. In addition to all these excellent physico-chemical properties, PDA yields sp^2-rich graphite like carbon upon carbonization under inert atmosphere at elevated temperatures. [28, 29]

In this work, we report the discovery of the 1T phase-enrichment and its stabilization within the MoS_2 nano-sheets, taking advantage of incorporation of in situ generated S-doped carbon. In this approach, the PDA-bound molybdate was pyrolyzed in presence of elemental sulfur. The obtained MoS_2@S-C_{PDA} exhibits excellent electrical conductivity, high crystallinity and more importantly, the formation of 1T phase with more edge planes. The MoS_2@S-C_{PDA} exhibited high electrocatalytic activity towards HER at low overpotential. Mo(VI) on polydopamine [Mo(VI)@PDA] was synthesized by mixing ammonium molybdate and dopamine (DA) resulting in an orange yellow colored DA-Mo(VI) complex.[30,31] FT-IR was used to characterize complex formation between DA and AM *via* hydrogen bonding or electrostatic interactions.[32,33] [Figure S1 ESI†]. The Mo(VI)@PDA was pyrolyzed at 1000°C under Ar in presence of elemental sulfur to yield MoS_2@S-C_{PDA}.

From the FESEM images (Figure 1a) of MoS_2 and MoS_2@S-C_{PDA}, it is evident that MoS_2 is mainly made of both particles and sheets whereas, the MoS_2@S-C_{PDA} has sheets stacked together. We further investigated the morphology by using TEM. Figure 1b shows the TEM images of MoS_2 and MoS_2@S-C_{PDA} that are in agreement with FESEM images of MoS_2 displaying particulate morphology with an average particle size of ~ 100 nm whereas,MoS_2@S-C_{PDA} shows a few or more wrinkled sheets. In order to assess the crystal structure X-ray diffraction (XRD) measurements were performed. Figure 2a compares the diffraction patterns of MoS_2 and MoS_2@S-C_{PDA}. The XRD pattern of MoS_2 shows crystalline reflections at 14.44^0 (002), 32.97^0 (101), 39.90^0 (103), 49.58^0 (105) and 60.70^0 (111) and MoO_3 at 26.21^0 (021), 37.16^0 (131), 53.77^0 (080), 66.70^0 (270). On the other hand, MoS_2@S-C_{PDA} displays a nominal shift of the reflection at 14.44^0 (002) towards lowerangles indicating an increase in the interlayer spacing from 6.14 to 6.41Å due to layer expansion and the presence of defects in MoS_2sheets.[34,35] Also, MoS_2@S-C_{PDA} was

found to be nanocrystalline with considerable increase in *fwhm* compared to its native counterpart.

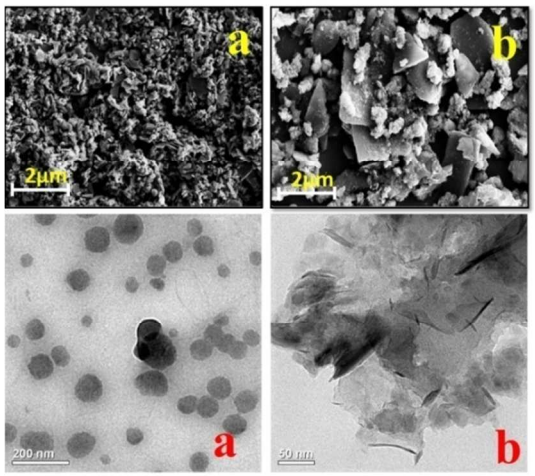

Figure 1: FESEM and TEM images of (a) MoS_2 and (b) MoS_2@S-C_{PDA} [Scale bars for TEM: (a) 200 nm; (b) 50 nm]

The stack height along the *c-axis* was estimated for MoS_2 and MoS_2@S-C_{PDA}using Scherrer equation and found to be 25 and 16.7 nm respectively indicating that MoS_2 exists as a few layers in MoS_2@S-C_{PDA}.[36] As expected, sulfide PDA-derived carbon (S-C_{PDA}) is found to be nanocrystalline with its characteristic peak at 25^0(Figure S2 ESI†). To confirm the presence of carbon and defects, Raman spectra were acquired for MoS_2 and MoS_2@S-C_{PDA} (Figure 2b). As expected both the spectra show well-defined peaks of MoS_2 at 410 and 384 cm^{-1} attributed to A_{1g} and E^1_{2g} bands respectively. In addition to the characteristic MoS_2 peaks, MoS_2@S-C_{PDA} displayed D and G bands at 1384 and 1560 cm^{-1} ascribed to the presence of carbon formed from PDA (Figure S3 ESI†). A minimal decrease in Δν of A1g and E^1_{2g} in MoS_2@S-C_{PDA} (25 cm^{-1}) compared to MoS_2 (28 cm^{-1}) suggests that MoS_2 exists as sheets in MoS_2@S-C_{PDA}.[37] A low intense and broad E^1_{2g} band of MoS_2@S-C_{PDA} compared to MoS_2 indicates defects arising from the presence of unsaturated sulfur at the edge planes.[38, 39]

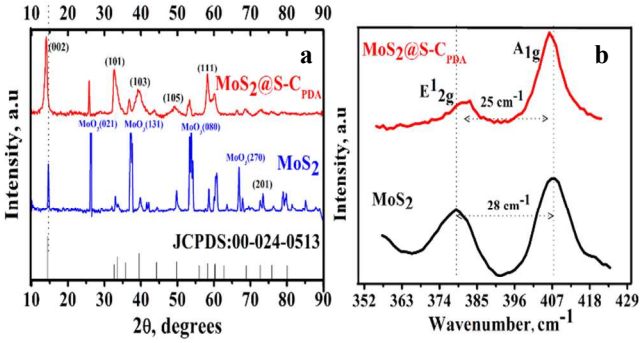

Figure 2: (a) XRD and (b) Raman spectra of MoS_2 and MoS_2@S-C_{PDA}

The oxidation state and elemental analysis were carried out using X-ray photoelectron spectroscopy (XPS). The XPS survey spectrum of MoS_2 shows C, O, Mo, S peaks at the corresponding binding energies. The high resolution carbon spectrum of MoS_2@S-C_{PDA} (Figure3a) shows peaks at 284.37, 285.20 eV corresponding to C=C, C-C or C-H indicative of the presence of sp^2 and sp^3 carbon respectively. While a broad peak at 288.56 eV corresponds to the presence of O-C-O species, the additional peak observed at 286.19 eV arises due to the sulfur- bound carbon(C-S).[40,41] Furthermore in S_{2p} spectra, the peak at 163.9 eV is $2p_{3/2}$ of thiophene-S due to spin–orbit coupling and the peak at 168.0 eV is the oxide-bound sulfur species (C-SOO-C) confirming sulfur-doping in the PDA-derived carbon.[42] Further, FT-IR was used to confirm S-doping of the carbon matrix (Figure S4 ESI†). Both MoS_2@S-C_{PDA} and MoS_2 samples display their characteristic ν (Mo-S) peak at 462 cm^{-1}. Additionally, the appearance of new peaks at 902 and 1110 cm^{-1} attributed to δ(C-S) and δ(C=S) respectively in the MoS_2@S-C_{PDA} spectra is a clear confirmation of attachment of sulfur to the carbon skeleton. FTIR spectra of S- doped carbon also show peaks of δ(C-S) and δ(C=S) similar to MoS_2@S-C_{PDA}.[43]

Deconvoluted Mo peak of MoS_2 sample shows that Mo is in (IV) oxidation state with binding energies of 229.30, 232.45 eV corresponding to $3d_{5/2}$, $3d_{3/2}$ respectively. The peak located at 235.0 eV can be attributed to the presence of Mo-O bond with Mo (VI) oxidation state.[21, 35] Deconvoluted sulfur peak shows a doublet at 161.55 eV for $S_{2p3/2}$ and 162.77 eV for $S_{2p1/2}$ confirming the presence of sulfide species, S_2^- (Figure S5 ESI†). The stoichiometric ratio of Mo:S in MoS_2 and MoS_2@S-C_{PDA} samples is found to be ~2. Interestingly, in MoS_2@S-C_{PDA}, a shift of 0.6 eV is observed in the binding energies of Mo (228.71 and 231.79 eV) and S (161.55, 162.77 eV). The shift in the binding energies implies the emergence of both 1T- and 2H-phases owing to the incorporation of S-doped carbon between the MoS_2 sheets resulting in layer expansion, as is also evident from an increase in the interlayer spacing (Figure 2a).[21,44] From the structural and chemical evaluation of MoS_2@S-C_{PDA}, it is reasonable to conclude that S-doped carbon is incorporated between MoS_2 sheets resulting in the transformation of 2H (semiconducting) to 1T phase (metallic) with more unsaturated sulfur atoms at the edges thereby increasing the number of active sites, for instance in electrocatalysis. Besides, structural modification and electronic modulation are known to play vital roles in the design of electrocatalysts.

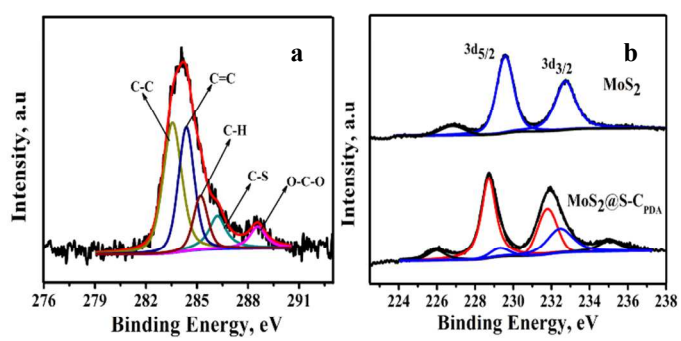

Figure 3: High resolution x-ray photoelectron spectra of (a) C_{1s} and (b) Mo_{3d} in MoS_2@S-C_{PDA}

Incorporation of heteroatoms between the MoS_2 nano-sheets in a controlled manner results in increased intrinsic conductivity and charge density.[45,36] Analogously, the band gaps of MoS_2 and MoS_2@S-C_{PDA} were determined using diffuse reflectance spectroscopy (DRS) to be 1.32 (indirect) and ~1.68 eV (direct) respectively (Figure S6). Bulk MoS_2 is well-known to show an indirect band gap of ~1.2 eV and single layer MoS_2 displays a direct band gap of ~ 1.8 eV. [46] It has been predicted that double and triple layers of MoS_2 show reduced band gap values of ~ 1.65 and 1.35 eV relative to a single layer MoS_2 suggesting that MoS_2@S-C_{PDA} consists of two layers (FigureS6 ESI†).[47] Furthermore, the band gap transition is well supported by UV-visible spectra (Figure S7 ESI†). Absorption spectra of MoS_2 and MoS_2@S-C_{PDA} display A and B

excitonic bands at 634 (1.95 eV), 687 nm (1.80 eV) respectively, corresponding to K and K´ of the Brillouin zone. In addition to K and K' bands, a broad peak at ~400 nm with two shoulder peaks at 398 and 448 nm were observed for MoS_2@S-C_{PDA} which can be ascribed to the direct transition of deep valence band to the conduction band.[48] A blue shift in A and B exciton bands in MoS_2@S-C_{PDA} can be attributed to the quantum-size confinement. Overall, the incorporation of S-doped carbon between MoS_2 sheets results in structural and electronic modification which is expected to favour enhancement in the hydrogen evolution reaction kinetics.

In order to evaluate the electrocatalytic activity of MoS_2@S-C_{PDA}, HER was performed in 0.5 M H_2SO_4 solutions using linear sweep voltammetry with a conventional 3-electrode setup. Figure 4a compares the linear sweep voltammograms of S-C_{PDA}/GC, MoS_2/GC, MoS_2@S-C_{PDA}/GC electrodes and benchmark Pt. MoS_2/GC and S-C_{PDA}/GC are active to HER at higher overpotentials (η > 300 mV), whereas MoS_2@S-C_{PDA}/GC shows onset of catalytic current at 60 mV vs RHE. As in the case of other MoS_x-based electrocatalysts, the present system is relatively closer to the performance of Pt in terms of proximity of the onset potential. The Tafel slopes determined from the linear region of the polarization curves for S-C_{PDA}, MoS_2 and MoS_2@S-C_{PDA} are found to be 180, 90 and 72 mV/decade respectively (inset in Figure 4a). However, as the mechanism of HER on MoS_2 surface is still not clearly understood, it is difficult to relate Tafel slopes to any mechanism readily.[8] In general, there are three steps proposed for HER in acidic medium, first step being the discharge step (Volmer reaction). The second step is either followed by surface atom (Tafel reaction) or ion-atom recombination (Heyrovsky reaction).[49] If the Tafel slope is 30 mV/decade, HER takes place via Volmer-Tafel or if it is above 40 mV/decade, it follows Volmer-Heyrovsky mechanism. In the present work, the HER on MoS_2@S-C_{PDA} shows a Tafel slope of 72 mV/decade suggesting Volmer-Heyrovsky mechanism. Similarly, the exchange current density (j_o) calculated for MoS_2@S-C_{PDA} is found to be 3.16×10^{-4} Acm^{-2} whereas, MoS_2 exhibited a value of 5.52×10^{-5} Acm^{-2} suggesting the presence of more active sites due to the presence of unsaturated sulfur atoms at the edge planes.

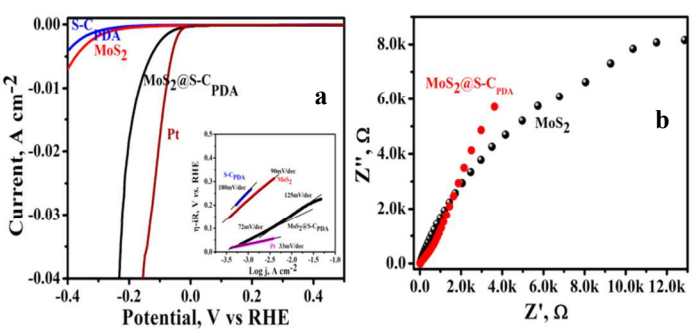

Figure 4: (a) Linear sweep voltammograms of MoS_2@S-C_{PDA}, MoS_2 and S-C_{PDA} modified electrodes in 0.5M H_2SO_4 (scan rate 2 mV/sec)(b) Impedancespectra of MoS_2@S-C_{PDA} and MoS_2 samples at overpotential of 150 mV. Electrolyte: 0.5M H_2SO_4. Frequency range: 1MHz-50 mHz. Amplitude: 10 mV

Additionally, the current density measured at a constant overpotential of 200 mV for MoS_2@S-C_{PDA} shows 18-fold increase (20 mA cm^{-2}) compared to MoS_2 (0.7 mA cm^{-2}). It is evident from Table S1that HER activity in terms of onset potential and exchange current density is superior to that of the other carbon-supported MoS_2 nano-sheets. [13-15, 35] In support of this observation, higher exchange current density and current density calculated at a constant overpotential indicates superior electrocatalytic activity of MoS_2@S-C_{PDA} relative to its counterparts. At the same time, it needs to be noted that MoS_2@S-C_{pDA} exhibits a lower current density at 200 mV relative to other carbon-supported systems which may be due to: (i) the lower conductivity of pDA-derived carbon compared to the graphene substrates; (ii) limited electron conduction compared to the graphene substrates [2]; and (iii) surface area of the pDA-derived carbon being lower than the nanoscopic graphene sheets.

Furthermore, to elucidate charge transport, interfacial charge transfer resistance (R_{ct}) values for MoS_2@S-C_{PDA}, MoS_2 are measured using electrochemical impedance spectroscopy at an overpotential of 150 mV (Figure 4b). The MoS_2@S-C_{PDA} and MoS_2 electrode shows R_{ct} values of 900 Ω and 8 kΩ respectively. Significant decrease in R_{ct} of MoS_2@S-C_{PDA} can be reasoned to the incorporation of sulfur- doped carbon aiding efficient charge transport. Stability of the electrode materials is one of the key parameters in determining the efficiency of electrocatalysts. Cyclic voltammetric experiments were performed in the potential range between the -0.3 to 0.2 V in acidic medium to evaluate the catalyst stability (Figure S8 ESI†). Even after 1000 cycles MoS_2@S-C_{PDA} electrode is able to retain its catalytic activity with a negligible decrease in the cathodic current.

Mechanistically, enhancement in the electrocatalytic activity may involve interplay of factors such as: (a) insertion of sulfur doped carbon between MoS_2 layers results in the MoS_2 structural rearrangements like layer expansion (confirmed by the d-spacing values in XRD) and also aids the 2H-1T phase transformation (as confirmed by XPS data). These studies reveal that MoS_2@S-C_{PDA} is enriched with unsaturated sulfur atoms at the edge sites; (b) this also brings about increased intrinsic electronic conductivity of MoS_2 nano-sheets that is reflected in the band gap changes. These structural and electronic rearrangements are in agreement with the previously reported density functional theoretical calculations performed on superlattices composed of graphene and MoS_2 layers [50] and (c) MoS_2@S-C_{PDA} exhibits metallic character due to increased charge transport between atomic layers, indicating a weak ionic interaction between the sulfur doped carbon and the MoS_2 layers similar to van der Waals forces. This can be attributed to high charge density of the sulfur doped carbon, contributing to increased electronic conductivity. It is well known that electronic modification along with the creation of more defective or edge sites is beneficial to the enhanced HER electrocatalysis.

In conclusion, a simple two step synthetic protocol is developed by immobilizing PDA on Mo precursor through complexation followed by pyrolysis in presence of elemental sulfur yielding alternate layers of S-doped carbon and MoS_2 nano-sheets. Incorporation of S-doped carbon between MoS_2 nano-sheets leads to layer expansion resulting in structural and electronic modifications. The key factors such as the number of active sites (unsaturated sulfur atoms at the edge planes) and electrical conductivity required for HER are simultaneously achieved by incorporation of S-doped carbon. The MoS_2@S-C_{PDA} displayed HER activity with a minimal onset potential of 60 mV vs. RHE with η = 160 mV@10 mA cm^{-2}. With this promising feature in mind, one may apply the present approach to other chalcogenides and compositional variations in order to achieve optimized catalytic performance. Further reduction in overpotential and enhancement in the current density may be possible by controlling the thickness of the doped carbon layers and in turn the electronic conductivity.

Notes and references

[a] Mr.Thangavel Naresh Kumar, Dr. Lakshminarasimha Phani Kanala
Nanoscale Electrocatalysis Group,
Electrodics & Electrocatalysis Division,
CSIR-Central Electrochemical Research Institute
Karaikudi 630006
Fax: (+) 914565227779, 227713
E-mail: kanalaphani@yahoo.com; klnphani@cecri.res.in

[b] Dr.Naveen Chandrasekaran
Electroplating & Metal Finishing Technology Division
CSIR-Central Electrochemical Research Institute, Karaikudi-06

Acknowledgements: TNK thanks India's CSIR for Senior research fellowship. KLNP acknowledges support from India's DST for a grant under Australia-India Strategic Research Fund [DST/INT/AUS/P-43/2011] and CSIR program under MULTIFUN: CSC-0101.

[Electronic supplementary information are available: Chemicals, experimental procedure, characterization such as FTIR, XRD, XPS, Laser Raman, DRS, UV-visible and comparison table data. See DOI: 10.1039/c000000x]

1. M. S. Dresselhaus, I. L. Thomas, *Nature* 2001, **414**, 332.
2. L. Chen, *J. Electrochem. Soc.*1991, **138**, 3321.
3. D. Das, *Int. J. Hydrogen Energy* 2001, **26**, 13.
4. X. Huang, Z. Zeng, H. Zhang, *Chem. Soc. Rev.* 2013, **42**, 1934.
5. X. Chen, S. Shen, L. Guo, S. S. Mao, *Chem. Rev.* 2010, **110**, 6503.
6. V. Fourmond, P. A. Jacques, M. Fontecave, V. Artero, *Inorg. Chem.* 2010, **49**, 10338.
7. P.-A. Jacques, V. Artero, J. Pécaut, M. Fontecave, *Proc. Natl. Acad. Sci. U. S. A.* 2009, **106**, 20627.
8. A. B. Laursen, S. Kegnæs, S. Dahl, I. Chorkendorff, *Energy Environ. Sci.* 2012, **5**, 5577.
9. T. Wang, L. Liu, Z. Zhu, P. Papakonstantinou, J. Hu, H. Liu, M. Li, *Energy Environ. Sci.* 2013, **6**, 625.
10. H. Liu, D. Su, R. Zhou, B. Sun, G. Wang, S. Z. Qiao, *Adv. Energy Mater.* 2012, **2**, 970.
11. Y. Shi, Y. Wan, R. Liu, B. Tu, D. Zhao, *J. Am. Chem. Soc.* 2007,**129**, 9522.
12. Z. Chen, D. Cummins, B. N. Reinecke, E. Clark, M. K. Sunkara, T. F. Jaramillo, *Nano Lett.* 2011, **11**, 4168.
13. D. Merki, S. Fierro, H. Vrubel, X. Hu, *Chem. Sci.* 2011, **2,** 1262.
14. A. Enyashin, L.Yadgarov, L. Houben, I. Popov, M. Weidenbach, R. Tenne, M.B. Sadan, G. Seifert, *J.Phys.Chem.C.* 2011, **115,** 24586.
15. Y.H. Chang, C.T. Lin, T.Y. Chen, C.L. Hsu, Y.H. Lee, W. Zhang, K.H. Wei, L.J. Li, *Adv. Mater.* 2013, **25,** 756.
16. Y. Li, H. Wang, L. Xie, Y. Liang, G. Hong, H. Dai, *J. Am. Chem. Soc.* 2011, **133**, 7296.
17. L. Liao, J. Zhu, X. Bian, L. Zhu, M. D. Scanlon, H. H. Girault, B. Liu, *Adv. Funct. Mater.* 2013, **23**, 5326.
18. M. a Lukowski, A. S. Daniel, F. Meng, A. Forticaux, L. Li, S. Jin, *J. Am. Chem. Soc.* 2013, ***135*,** 10274.
19. J. Xiao, D. Choi, L. Cosimbescu, P. Koech, J. Liu, J. P. Lemmon, *Chem. Mater.* 2010, **22,** 4522.
20. T. F. Jaramillo, K. P. Jørgensen, J. Bonde, J. H. Nielsen, S. Horch, I. Chorkendorff, *Science.* 2007, **317,** 100.
21. H. Wang, Z. Lu, S. Xu, D. Kong, J. J. Cha, G. Zheng, P.-C. Hsu, K. Yan, D. Bradshaw, F. B. Prinz, et al., *Proc. Natl. Acad. Sci. U. S. A.*2013, **110,** 19701.
22. H. Lee, S. M. Dellatore, W. M. Miller, P. B. Messersmith, *Science* 2007, **318**, 426.
23. Q. Ye, F. Zhou, W. Liu, *Chem. Soc. Rev.* 2011, ***40*,** 4244.
24. D. R. Dreyer, D. J. Miller, B. D. Freeman, D. R. Paul, C. W. Bielawski, *Langmuir* 2012, **28,** 6428.
25. J. Liebscher, R. Mrówczyński, H. Scheidt, C. Filip, N. D. Hădade, R. Turcu, A. Bende, S. Beck, *Langmuir* 2013, ***29*,** 10539.
26. S. M. Kang, S. Park, D. Kim, S. Y. Park, R. S. Ruoff, H. Lee, *Adv. Funct. Mater.* 2011, **21**, 108.
27. B. Fei, B. Qian, Z. Yang, R. Wang, W. C. Liu, C. L. Mak, J. H. Xin, *Carbon N. Y.* 2008, **46**, 1795.
28. R. Li, K. Parvez, F. Hinkel, X. Feng, K. Müllen, *Angew. Chem. Int. Ed. Engl.* 2013, **52**, 5535.
29. X. Yu, H. Fan, Y. Liu, Z. Shi, Z. Jin, *Langmuir* 2014, **30**, 5497.
30. C. Zhao, J. Kong, L. Yang, X. Yao, S. L. Phua, X. Lu, *Chem. Commun. (Camb).* 2014, **50,** 9672.
31. Midway through our work, MoS_2-supported on dopamine-derived carbon was reported by Zhao et al [X. Lu*et.al., Chem. Commun.,* 2014, **50**, 9672] that is bereft of any structural and electronic modifications to MoS_2
32. H. Li, Y. Jia, A. Wang, W. Cui, H. Ma, X. Feng, J. Li, *Chemistry* 2014, **20**, 499.
33. L. X. Song, M. Wang, Z. Dang, F. Y. Du, *J. Phys. Chem. B* 2010, **114**, 3404.
34. L. Yang, X. Cui, J. Zhang, K. Wang, M. Shen, S. Zeng, S. a Dayeh, L. Feng, B. Xiang, *Sci. Rep.* 2014, **4**, 5649.
35. Y. Yan, B. Xia, X. Ge, Z. Liu, J.Y. Wang, X. Wang, *ACS Appl. Mater. Interfaces* 2013, **5**, 12794.
36. J. Xie, H. Zhang, S. Li, R. Wang, X. Sun, M. Zhou, J. Zhou, X. W. D. Lou, Y. Xie, *Adv. Mater.* 2013, **25**, 5807.
37. D. Y. Chung, S.-K. Park, Y.H. Chung, S.-H. Yu, D.-H. Lim, N. Jung, H. C. Ham, H.Y. Park, Y. Piao, S. J. Yoo, et al., *Nanoscale* 2014, **6**, 2131.
38. Y. Yan, X. Ge, Z. Liu, J.-Y. Wang, J.-M. Lee, X. Wang, *Nanoscale* 2013, **5,** 7768.
39. K.K. Liu, W. Zhang, Y.H. Lee, Y.C. Lin, M.T. Chang, C.Y. Su, C.S. Chang, H. Li, Y. Shi, H. Zhang, et al., *Nano Lett.* 2012, **12**, 1538.
40. J. P. Paraknowitsch, A. Thomas, J. Schmidt, *Chem. Commun. (Camb).*2011, **47**, 8283.
41. D. Zhang, Y. Hao, L. Zheng, Y. Ma, H. Feng, H. Luo, *J. Mater. Chem. A* 2013, ***1*,** 7584.
42. X. Li, S. P. Lau, L. Tang, R. Ji, P. Yang, *Nanoscale* 2014, **6**, 5323.
43. Y. Xia, *Carbon N. Y.*2012, **50**, 5543.
44. G. Eda, H. Yamaguchi, D. Voiry, T. Fujita, M. Chen, M. Chhowalla, *Nano Lett.* 2011, **11**, 5111.
45. J. Xie, J. Zhang, S. Li, F. Grote, X.Zhang, H.Zhang, R.Wang, Y.Lei, B.Pan, Y.Xie, *J.Am.Chem.Soc.* 2013, **135,** 17881.
46. B. Radisavljevic, A. Radenovic, J. Brivio, V. Giacometti, A. Kis, *Nat. Nanotechnol.* 2011, **6**, 147.
47. H. S. Lee, S.W. Min, Y.G. Chang, M. K. Park, T. Nam, H. Kim, J. H. Kim, S. Ryu, S. Im, *Nano Lett.* 2012, **12**, 3695.
48. J. Wilcoxon, G. Samara, *Phys. Rev. B* 1995, **51**, 7299..
49. L. A Kibler, *ChemPhysChem* 2006, **7**, 985.
50. X.D.Li, S.Yu, S.Q.Wu,Y.H.Wen, S.Zhou, Z.Z.Zhu, *J.Phys.Chem.C* 2013, **117**, 15347-15353